A Control Architecture to Coordinate Renewable Energy Sources and Energy Storage Systems in Islanded Microgrids

Wu, Dan; Tang, Fen; Dragicevic, Tomislav; Vasquez, Juan C.; Guerrero, Josep M.

Published in:
I E E E Transactions on Smart Grid

DOI (link to publication from Publisher):
10.1109/TSG.2014.2377018

Publication date:
2015

Document Version
Early version, also known as pre-print

A Control Architecture to Coordinate Renewable Energy Sources and Energy Storage Systems in Islanded Microgrids

Dan Wu, Fen Tang, Tomislav Dragicevic, Juan C. Vasquez, Josep M. Guerrero

***Abstract*—Coordinated operation of microgrids requires that energy management system takes into account both the available power in renewable energy sources (RES) and storage capacity of energy storage systems (ESS). In this paper, a coordinated architecture of islanded AC microgrids with smooth switching droop control (SSDC) is derived. Based on the proposed SSDC approach, flexible power control of each ESS /RES unit can be obtained with seamless modes changes. Furthermore, decentralized power management can be achieved by executing frequency bus-signaling (FBS). The power management principle based on different operational modes is explained in details, and small-signal analysis is carried out for SSDC. Real-time hardware-in-the-loop (HiL) results of an islanded microgrid are provided under several scenarios to validate the proposed coordinated control strategy.**

***Index Terms*—Microgrids, coordinated operation, smooth switching droop control (SSDC), frequency bus-signaling (FBS).**

I. Introduction

NOWADAYS, distributed power systems are gaining a great attention due to the advantages such as being more reliable, easily scalable and flexibly controlled compared to the large centralized power systems. Microgrid is emerging as a potential concept to realize this distributed power system paradigm. Integrated with renewable energy sources (RES) and other distributed generation (DG), energy storage systems (ESS) and active loads, microgrids can operate in grid-connected mode to exchange power with main utility, or in islanded mode to supply local loads when the grid is not present [1]. Thanks to the rapid development of power electronics in recent years, RES such as photovoltaic (PV) systems and wind turbines (WT) systems are becoming major DG sources in microgrids. However, due to their intermittent nature, ESS systems are indispensable elements in microgrids that buffer the short-term unbalanced power between RES and load [2]. In previous works, several hybrid RES/ESS systems are developed [3], [4], while performance and purpose evaluation of different ESS technologies applied in DG systems is summarized in [5]. However, the capacity limitation of ESS is seldom considered in these works. Methodologies for prediction and optimal sizing of ESS are thereby developed [6]-[8]. Although these methods are effective to avoid the over-charge/over-discharge of ESS when the system capacity is deterministic, the ESS needs to be redesigned when the total energy generation/consumption is changed. In [9], a coordinated control strategy for PV systems and battery storage system is proposed, in which the power coordination takes into account both the available power in RES and SoC conditions of ESS. This control algorithm is suitable for PV systems with ESS integrated on DC link, but still needs additional control scheme to coordinate with other distributed microgrid elements that connected on AC bus side.

Therefore, in order to achieve flexible and reliable performance of microgrids, different power conditions of distributed RES and storage capacity of ESS need to be globally considered. An energy management algorithm based on model predictive control is proposed to coordinate DG and ESS units according to different DG power conditions [10], [11], while a coordinated state of charge (SoC) control strategy is derived in microgrids management systems to stabilize the bus frequency and voltage amplitude of microgrids [12], [13]. In these works, the coordinated operation between ESS and RES relies on the centralized management control, so that the overall system will lose coordination when a single point failure occurs in one of the communication links. Other advanced control algorithm can be found in i.e. [14]. With the proposed control strategy, flexible demand participation is considered in order to achieve decentralized microgrid coordination, but it needs complex computation and additional communication link is still mandatory.

In order to avoid using external communication links, autonomous control strategies for power distribution have been investigated. Power line communication methods are proposed to use AC/DC power line as communication channels for power management [15], [16]. For instance, coordinated control strategies are developed by using a range of high frequency components over power line communication carriers [17], [18], but this inherently introduces noise and the bandwidth of these signals should be well designed. Another similar approach is DC bus-signaling method using bus voltage levels as thresholds to schedule sources in DC

Dan Wu, Juan C. Vasquez, Josep M. Guerrero, are with Department of Energy Technology, Aalborg University, 9220 Aalborg (e-mail: dwu@et.aau.dk; juq@et.aau.dk; joz@et.aau.dk).

Fen Tang is with School of Electrical Engineering, Beijing Jiaotong University (e-mail: ftang_nego@126.com).

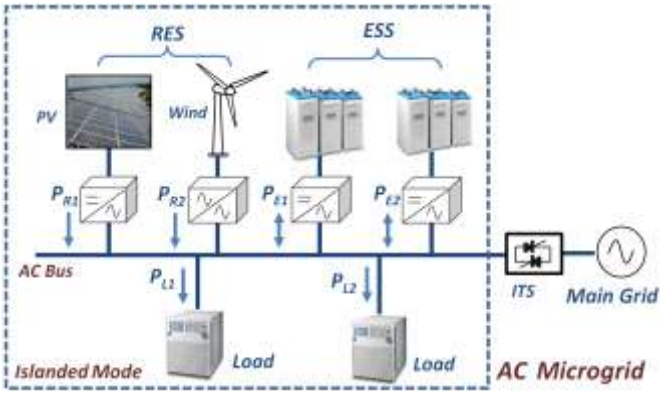

Fig. 1. Typical configuration of a AC microgrid.

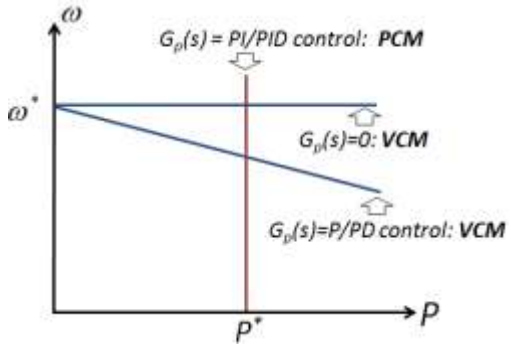

Fig. 2. Steady-state relation of ω-P based with different droop controllers.

microgrids [19], [20], while little work so far has been found in AC systems implementing this approach. Droop control strategy has been proposed to achieve desirable active and reactive power sharing in AC microgrids by regulating output frequency and voltage amplitude of each DG unit [21], [22], This coordinated performance mimics the inertia response of synchronous machine in large power systems, and can be implemented on parallel units under voltage control mode (VCM) in a decentralized way. However, since most of RES units are controlled in power control mode (PCM) at maximum power point (MPP), conventional droop method is difficult to be implemented directly for power management in integrated RES and ESS systems. Moreover, it is worth noticing that an adaptive droop control strategy is proposed in [23] for microgrid operating in either grid connected or islanded mode. Nevertheless, the DG conditions are not taken into consideration and overall system relies on external communication link to ensure different modes operation.

In this sense, this paper proposes a smooth switching droop control (SSDC) applied to RES/ESS units for their coordinated operation in islanded microgrids, which combines the advantages of both droop control and bus-signaling methods by achieving: i) automatic power sharing among VCM units and flexible power control of DG units with seamless transfer procedures; ii) decentralized power management according to power availability in RES and SoC of batteries in the ESS.

This paper is organized as follows. Section II gives a system configuration of AC microgrids and corresponding coordinated operation description. Section III illustrates SSDC principle and power management of system. Section IV describes the controller implementation. Section V depicts the small-signal stability analysis based on SSDC. Section VI shows the real-time hardware-in-the-loop (HiL) results under various scenarios in order to verify the proposed coordinated control based on SSDC. Finally, Section VII gives the conclusion.

II. Microgrid System Configuration

A typical configuration of an AC microgrid is shown in Fig. 1, where the microgrid operation is classified into grid-connected and islanded modes. When a fault occurs on the main grid, the intelligent transfer switch (ITS) disconnects the microgrid to enable the islanded operation. In this case the RES and ESS units are left on their own to provide the AC bus voltage and frequency support. In conventional way, the RES units perform as "grid-following" units and $P_{Ri(i=1,2)}$ are controlled at MPP to utilize maximum renewable energy. Meanwhile, ESS units perform as "grid-forming" components to fix the AC bus voltage and frequency, and provide the buffer power $P_{Ei(i=1,2)}$ ($\sum P_{Ei}=\sum P_{Li}-\sum P_{Ri}$) to microgrids automatically. Without power providing from the main grid, the ESS units take the sole role to balance power between renewable energy generation and loads consumption.

In islanded microgrids, the coordinated operation can be achieved by source scheduling among ESS and RES units, which targets at avoiding over-charge condition of ESS, and demand side management among ESS and local loads which focuses on avoiding over-discharge of ESS. In the former scenario, RES units are controlled in PCM at MPP, while ESS units are controlled in VCM when ESS is not fully charged. When ESS comes close to be fully charged, coordinated control strategy is required in order to ensure that the power charging to ESS is constrained ($P_{Ei(i=1,2)} \approx 0$) and works in PCM. At the same time, the power generated from RES decreases to match with the consumption of loads ($\sum P_{Ri} \approx \sum P_{Li}$), so that RES units then operate in VCM. Furthermore, if the loads suddenly increase consumption or RES units decrease generation, the coordinated control strategy should enable the ESS units to discharge power so that the overall system changes back to normal operation. Finally, for the latter scenario of demand side management, the principle of coordinated control among ESS units and loads can be similarly applied to source scheduling, but this issue is out of the scope of this paper.

In the literature, the power distribution among microgrid elements discussed above is usually achieved in a centralized way [24], [25]. In these works the microgrid utilizes master-slave control structure where the ESS under VCM and the RES under PCM are defined as master and slave units respectively [26]. Then, the distribution of power based on prime-source conditions is processed by a central controller which sends out reference signals through communication links. This method is widely used, but suffers from inherent single-point of failure and imposes serious limitations when there are a large number of spatially distributed elements. In the following Sections, a decentralized method for power

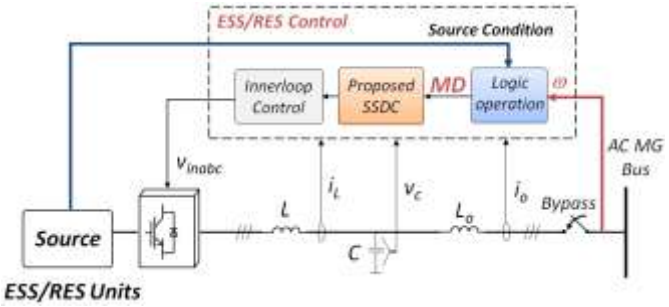

Fig. 3. Control scheme of ESS and RES based on SSDC.

regulation based on droop control strategy is illustrated, and with external communication link being removed compared with conventional master-slave control strategy.

III. Decentralized Coordinated Control Strategy

This Section targets at developing autonomous coordinated operation of islanded microgrids based on decentralized power control strategy for distributed units (RES/ESS).

A. Smooth Switching Droop Control

In order to regulate the output active and reactive power of each unit in a decentralized way, droop control is often used as follows [22]

$$\omega = \omega^* - G_P(s)(P_c - P^*) \quad (1)$$

$$E = E^* - G_Q(s)(Q_c - Q^*) \quad (2)$$

where G_P(s) and G_Q(s) denote the active and reactive power droop controller. P_c and Q_c are the measured active and reactive power of the unit, while P^* and Q^* are their references. The active power regulation based on G_P (s) with typical proportional (P)/proportional derivative (PD) control, and proportional integral (PI)/proportional integral derivative (PID) control is summarized in Table I, where that G_P (s) equals to zero can be treated as an ideal case of P droop control. The reactive power control can be similarly deduced. The values of these controllers reflect the slopes of ω-P curves which is presented in Fig. 2. In this way, control modes (PCM and VCM) can be flexibly switched by adjusting the slopes of ω-P curves. The SSDC droop control can be expressed as

$$G_P(s) = m_p + m_d s + \frac{m_i}{s} \cdot MD \quad MD \in [0,1] \quad (3)$$

$$G_Q(s) = n_p \quad (4)$$

where m_p, m_i and m_d are the parameters of PID droop controller for active power regulation, n_p is the coefficient for reactive power regulation, and *MD* is the trigger signal to control the integral term. Depending on the value of *MD*, each unit is able to operate in either VCM (*MD*=0) or PCM (*MD*=1). The control scheme of ESS and RES units based on SSDC is shown in Fig. 3, where the trigger signal *MD* is produced from logic operation block based on both source condition and bus frequency status. With proposed control strategy, *MD*=0 indicates that primary control operates under P droop, and *MD*=1 indicates operation under PI droop. There is also a low pass filter to smooth the changes between these two modes for each unit, which makes the signal continuously moving between 0 and 1.

TABLE I
Power Regulation Performance based on droop controllers

Droop Controller G_P(s)	P/PD control	PI/PID control	0
Control Mode	VCM	PCM	VCM
Output Power of i^{th} (j^{th}) unit	$\frac{P_i}{P_j} = \frac{m_{pj}}{m_{pi}}$	$P_i = P_i^*$	-

TABLE II
Operation Modes for ESS and RES Units

	Mode I	*Mode II*	*Mode III*	*Mode IV*
ESS	VCM ⇨	PCM	PCM ⇨	VCM
RES	PCM	PCM ⇨	VCM	VCM

In this paper, for deducing (1)-(4), the ratio of *X/R* is assumed to be high considering high reactance value of output filter. While in cases of low voltage distribution system, the resistance of line impedance can be dominant. In this sense the active power then needs to be regulated with *E-P* droop control [27], [28]. In that case, the corresponding bus-signaling method can then be similarly deduced based on bus voltage amplitude regulation with droop controller summarized in Table I. Finally, when the line the impedance under consideration is complex, advanced droop control that aims at decoupling the active and reactive power regulation with respect to bus frequency and voltage amplitude can be adopted as shown in [28].

B. Power Management Scheme based on SSDC

Apart from preserving the droop characteristic of autonomous power sharing among VCM units, another advantage of SSDC is executing frequency bus-signaling (FBS) to achieve decentralized power management, which indicates using bus frequency thresholds resulted from SSDC control to trigger modes changes. The coordinated operation of ESS and RES units can be categorized into four modes which are defined in Table II. The four operation modes are described as follows,

1) *Mode I*: In this mode, the islanded microgrid is in normal operation, and not all ESS are fully charged. At least one ESS is controlled in VCM to perform grid forming. The total storage system has capability to regulate power unbalance between generation and consumption. All RES units are controlled in PCM and inject constant power to the system.

2) *Mode II*: In this mode, all ESS units are near to be fully charged so they are controlled in PCM to limit charging power. Since we suppose there is no additional communication link to inform RES to change mode, the RES units still operate in PCM. The result of this control mode with all units operating in PCM is that the bus frequency increases since total power generation of system is larger than consumption ($\sum P_{Ri} > \sum P_{Li}$).

3) *Mode III*: In this control mode, the RES units are controlled in VCM as grid-forming units while ESS units are controlled in PCM to limit power. The process of changing modes of RES from PCM to VCM is accomplished when the

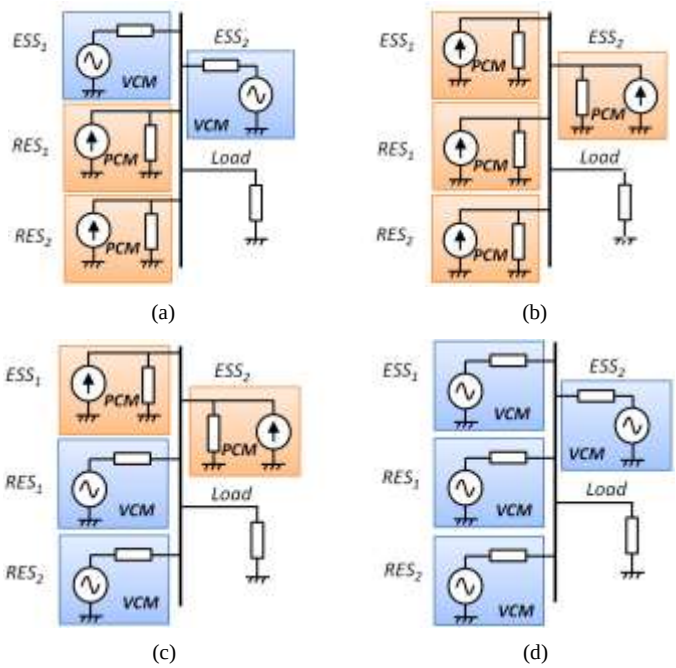

Fig. 4. Equivalent circuits of proposed system under different modes: (a) Mode I, (b) Mode II, (c) Mode III, and (d) Mode IV.

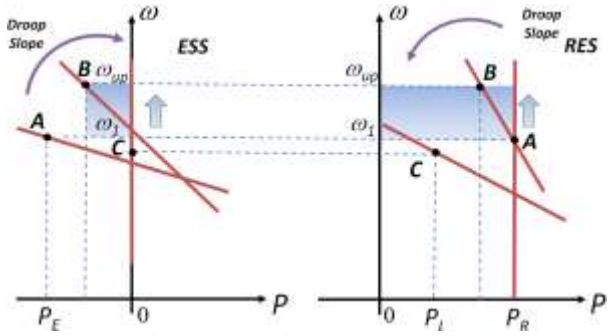

Fig. 5. Modes transferring process from Mode I to Mode III.

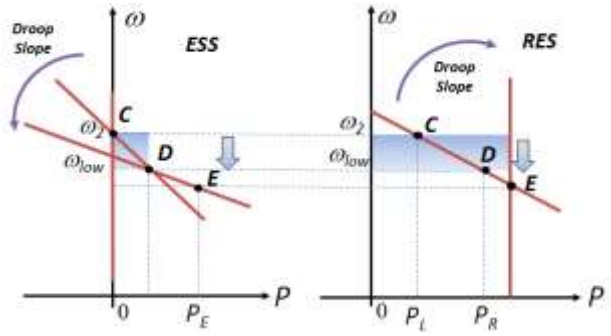

Fig. 6. Modes transferring process from Mode III to Mode I.

bus frequency reaches up threshold ω_{up}, which should be designed within the maximum frequency deviation as defined in different grid code.

4) *Mode IV*: In this control mode, the ESS units change back to VCM and cooperate with RES to share power consumption of loads. Similar as in Mode III, the mode changing procedure of ESS from PCM to VCM is accomplished when the bus frequency reaches a low-threshold ω_{low}. In this scenario, the power generation is lower than power consumption ($\sum P_{Ri} < \sum P_{Li}$) and ESS units start to discharge.

The equivalent circuits under different mode operations are summarized in Fig. 4. Among these four modes, the Mode I and Mode III are static modes in the proposed system which dominate major operation, while Mode II and Mode IV are dynamic modes to enable transferring between Mode I and Mode III by executing FBS.

The transferring process from Mode I to Mode III by adjusting the slopes of ω-P curves is shown in Fig. 5. At first, the system operates in Mode I so that the droop slopes of ESS and RES curves are constant and infinite respectively. The overall system operates at point *A*. When all ESS units are near to be fully charged, the trigger signal *MD* of ESS units is set as *MD*=1, and system transferred to Mode II. According to (3) with $P_c < P^*$, the bus frequency increases consequently by the integral effect. When the bus frequency reaches ω_{up} and system operates at point *B*, RES units are transferred to VCM by setting their trigger signal as *MD*=0 and the droop slope decreases to a constant value. Finally, the overall system gets stabilized at point *C* in Mode III where the slopes of ESS and RES curves are infinite and constant, respectively.

Fig. 6 shows the modes transferring process from Mode III back to Mode I with SSDC control. The overall system operates at point *C* in Mode III initially. When load increases, the bus frequency decreases consequently by droop control. When the output frequency decreases to a low-threshold ω_{low} at point *D*, ESS units change mode back to VCM by setting *MD*=0. The droop slope of ESS decreases to a constant value and system operates in Mode IV. When power provided by RES reaches at MPP, the RES units are controlled in PCM with *MD*=1. The overall system changes back to Mode I and operates at point *E*. It can be concluded that the coordinated control works in a circulate fashion, which is shown in Fig. 7. In Fig. 7, the selection of particular threshold SoC_u takes into the following considerations: i) the higher SoC_u selected, the more efficiently can the renewable energy from PV system be used. ii) SoC has an estimation error and should give a margin of over charge scenario [29]. Therefore, there is a trade-off between the safe operation of ESS in moderate SoC and efficient utilization of renewable energy. In this paper SoC_u=85% is considered, while in practical viewpoint it should be determined based on specific application requirements of ESS systems. A more detailed elaboration on selection of upper and lower SoC thresholds can be found in [30].

IV. Proposed Control Strategy Implementation

For each ESS and RES control system, the control structure can be classified into inner loop control and SSDC droop control. For inner loop control, proportional resonant (PR) controller is utilized to achieve good output voltage regulation. Additional virtual impedance is used to decouple the active and reactive power regulation. This inner loop control design can be referred to [21].

The SSDC based primary control algorithms for ESS and RES units are shown in Fig. 8. The ESS and RES units have the unified structure of droop control which includes PID

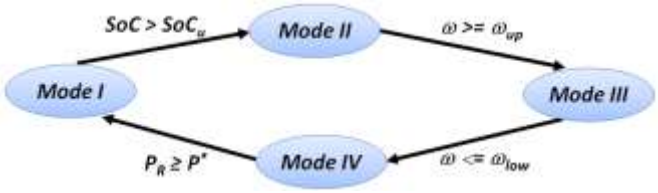

Fig. 7. Coordinated operation of system based on four modes .

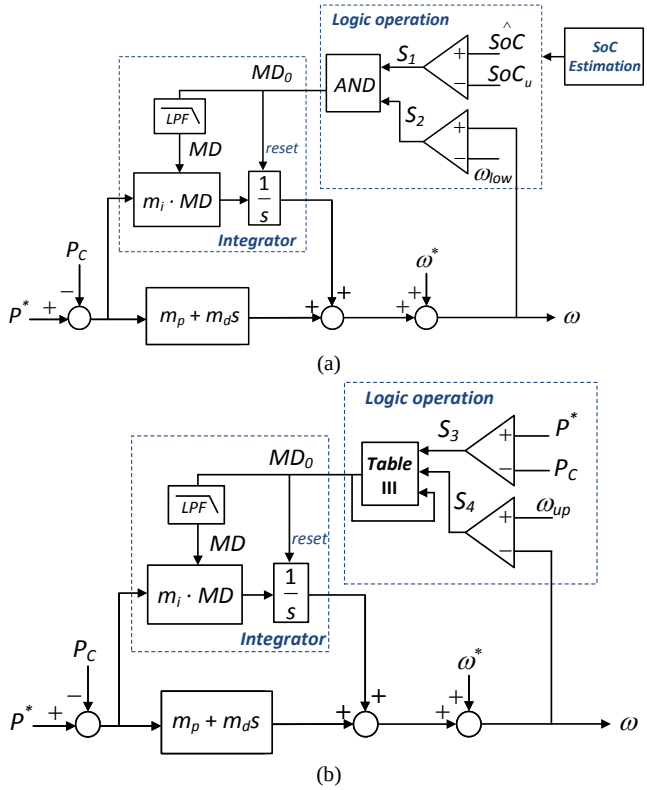

Fig. 8. SSDC control algorithms for ESS (a) and RES (b).

controller expressed in (3) and (4). The difference of these two types of controllers is the condition that changes the respective trigger signal *MD*. The low pass filter LPF in the integrator is used for smoothing the transition process between PCM and VCM modes, which is drawn from the output of logic operation MD_0. For the SSDC of ESS, the value of MD_0 is a "AND" operation of comparator output signals S_1 and S_2, which is shown in Fig. 8(a). The corresponding logic operation is shown as ESS logic of Table III. For the SSDC of RES shown in Fig. 8(b), the logic signal MD_{0n} not only depends on the comparators output S_3 and S_4, but also on the previous state MD_{0n-1}. The logic operation of SSDC for RES units is summarized as RES logic of Table III. In terms of frequency thresholds, the ω_{up} is selected higher than the maximum frequency threshold based on droop control when ESS units absorb total amount of power from RES units, in order to avoid unnecessary mode changes due to sudden load outage, not due to fully charged situation. The ω_{low} is selected equal to the nominal value of frequency in order to denote the overall system redraw from fully charged situation, since we have $\omega < \omega^*$ when ESS units start to discharge. In practice, a small voltage band can be added on this frequency threshold to give a margin for system dynamic regulation.

TABLE III
Logic Operation

ESS Logic			RES Logic			
S_1	S_2	MD_0	MD_{0n-1}	S_3	S_4	MD_{0n}
0	0	0	0	0	X	1
0	1	0	0	1	X	0
1	0	0	1	X	0	0
1	1	1	1	X	1	1

Note: X is irrelevant condition, which can be either in 0 or 1.

V. Small-Signal Analysis

In order to investigate the dynamic stability of electrical power systems, small-signal analysis is usually carried out. Based on classical control theory, a set of differential equations describing the system can be written in state space form as

$$[\dot{x}] = A[x] \tag{5}$$

where A is the state space matrix and $[x]$ is the state space vector. The dynamic properties of system's response can be analyzed by the characteristic equation

$$|sI - A| = 0 \tag{6}$$

In this sense, this paper gives the process of constructing matrix A based on SSDC method and analyzes the stability though root locus plots by deducing the eigenvalues of (6).

The active and reactive power delivered from the converter to the AC microgrid bus through inductive output impedance can be deduced as [31],

$$P = \frac{3}{2}\cdot\frac{EV}{X}\sin\phi \tag{7}$$

$$Q = \frac{3}{2}\cdot\frac{EV\cos\phi - V^2}{X} \tag{8}$$

where E and V are the output voltage amplitude and common bus voltage amplitude respectively, P and Q are the instantaneous active and reactive power, ϕ is the power angle of the output voltage, X is the reactance of output impedance. Considering small disturbances around the stable equilibrium point $\{\phi_e, E_e, V_e\}$ and linearize (7) and (8), we have

$$\Delta P = \frac{\partial P}{\partial E}\Delta E + \frac{\partial P}{\partial \phi}\Delta\phi = \alpha_1\Delta E + \alpha_2\Delta\phi \tag{9}$$

$$\Delta Q = \frac{\partial Q}{\partial E}\Delta E + \frac{\partial Q}{\partial \phi}\Delta\phi = \beta_1\Delta E + \beta_2\Delta\phi \tag{10}$$

Where α_1, α_2, β_1, β_2 are the partial derivatives calculated from (7) and (8), which are expressed as

$$\alpha_1 = \frac{3}{2}\cdot\frac{V\sin\phi}{X}, \quad \alpha_2 = \frac{3}{2}\cdot\frac{EV\cos\phi}{X} \tag{11}$$

$$\beta_1 = \frac{3}{2}\cdot\frac{V\cos\phi}{X}, \quad \beta_2 = -\frac{3}{2}\cdot\frac{EV\sin\phi}{X} \tag{12}$$

On the other hand, by linearizing droop control (1) and (2), we obtain following expressions

$$\Delta\omega = -G_P(s)\cdot\frac{\omega_c}{s+\omega_c}\Delta P \tag{13}$$

$$\Delta E = -G_Q(s)\cdot\frac{\omega_c}{s+\omega_c}\Delta Q \tag{14}$$

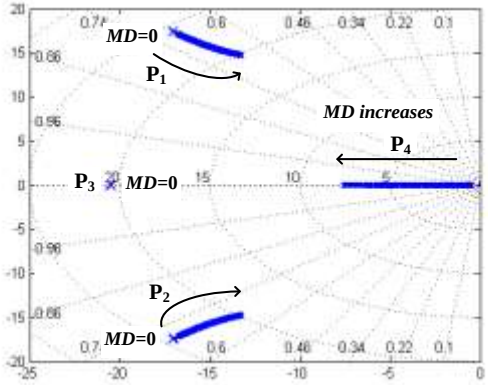

Fig. 9. Root locus diagram for MD=0 and 0<MD≤1.

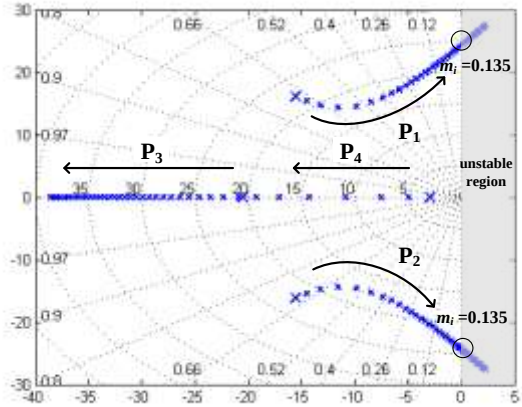

Fig. 10. Root locus diagram for 0.01≤mi≤0.2 (MD=1).

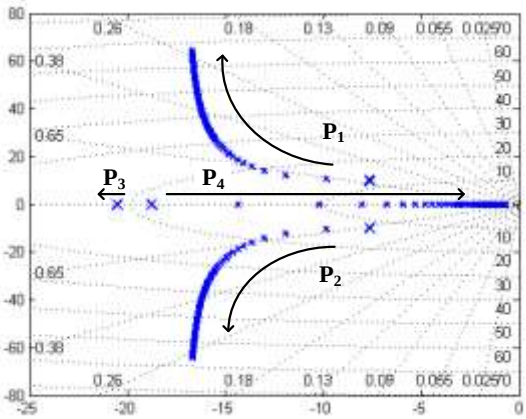

Fig. 11. Root locus diagram for 0.003≤m_p≤0.03 (*MD*=1).

where ω_c is cut off frequency of the low pass filter measuring *P* and *Q*. Supposing *MD*≠0 and taking (3) and (4) into (13), the following dynamic equation can be constructed

$$\Delta\ddot{\omega} = -\omega_c\Delta\dot{\omega} - \omega_c m_d\Delta\ddot{P} - \omega_c m_p\Delta\dot{P} - \omega_c m_i MD\Delta P \qquad (15)$$

$$\Delta\dot{E} = -\omega_c\Delta E - n_p\omega_c\Delta Q \qquad (16)$$

The differential terms of active power in (15) can be deduced from (9) considering partial derivatives are constants,

$$\Delta\dot{P} = \alpha_1\Delta\dot{E} + \alpha_2\Delta\omega \qquad (17)$$

$$\Delta\ddot{P} = \alpha_1\Delta\ddot{E} + \alpha_2\Delta\dot{\omega} \qquad (18)$$

Taking (10) into (16), we have

$$\Delta\dot{E} = \beta_3\Delta\phi + \beta_4\Delta E \qquad (19)$$

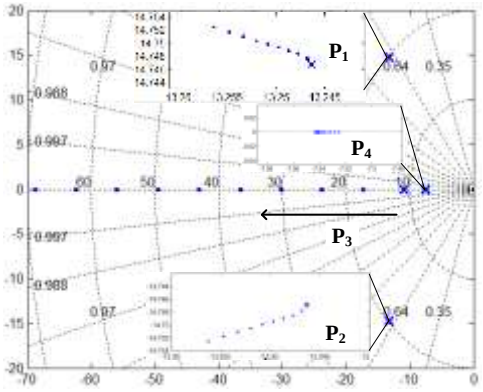

Fig. 12. Root locus diagram for 0.01≤n_p≤0.1 (*MD*=1).

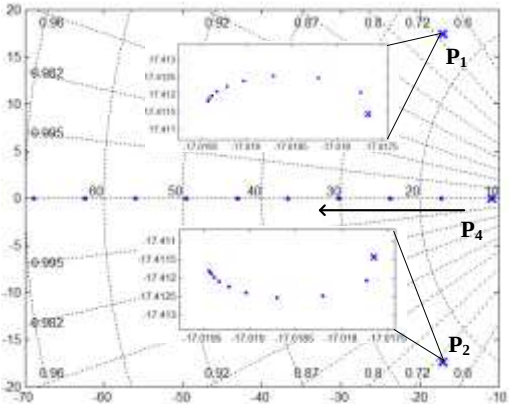

Fig. 13. Root locus diagram for 0.01≤n_p≤0.1 (*MD*=0).

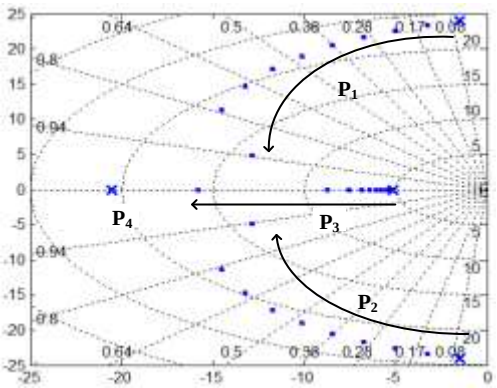

Fig. 14. Root locus diagram for 0.000025≤m_d≤0.00025 (*MD*=1).

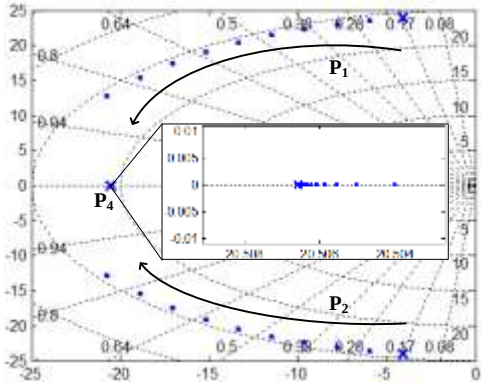

Fig. 15. Root locus diagram for 0.000025≤m_d≤0.00025 (*MD*=0).

$$\Delta\ddot{E} = \beta_3\beta_4\Delta\phi + \beta_3\Delta\omega + \beta_4{}^2\Delta E \qquad (20)$$

where β_3 and β_4 are defined as

$$\beta_3 = -n_p\omega_c\beta_2, \quad \beta_4 = -(\omega_c + n_p\omega_c\beta_1) \tag{21}$$

Taking (17)-(20) into (15), (15) can be rewritten as

$$\Delta\ddot{\omega} = a_{11}\Delta\dot{\omega} + a_{12}\Delta\omega + a_{13}\Delta\phi + a_{14}\Delta E \tag{22}$$

where the constant a_{11}, a_{12}, a_{13} and a_{14} are

$$a_{11} = -\omega_c(1 + m_d\alpha_2) \tag{23}$$

$$a_{12} = -\omega_c\left(m_p\alpha_2 + m_d\alpha_1\beta_3\right) \tag{24}$$

$$a_{13} = -\omega_c\left[\alpha_1\beta_3(m_p + m_d\beta_4) + m_i MD\alpha_2\right] \tag{25}$$

$$a_{14} = -\omega_c\left(m_p\alpha_1\beta_4 + m_i MD\alpha_1 + m_d\beta_4{}^2\right) \tag{26}$$

Define the state vector as

$$[x] = \left[\Delta\dot{\omega} \quad \Delta\omega \quad \Delta\phi \quad \Delta E\right]^T \tag{27}$$

And combine (19) and (22) in the form of (5), we have

$$A = \begin{bmatrix} a_{11} & a_{12} & a_{13} & a_{14} \\ 1 & 0 & 0 & 0 \\ 0 & 1 & 0 & 0 \\ 0 & 0 & \beta_3 & \beta_4 \end{bmatrix} \tag{28}$$

In the case of *MD*=0, the dynamic equation of (22) can be turned into

$$\Delta\dot{\omega} = a'_{11}\Delta\omega + a'_{12}\Delta\phi + a'_{13}\Delta E \tag{29}$$

where the constant a'_{11}, a'_{12} and a'_{13} are

$$a'_{11} = -\omega_c(m_d\alpha_2 + 1) \tag{30}$$

$$a'_{12} = -\omega_c\left(m_d\alpha_1\beta_3 + m_p\alpha_2\right) \tag{31}$$

$$a'_{13} = -\omega_c\left(m_d\alpha_1\beta_4 + m_p\alpha_1\right) \tag{32}$$

Define the state vector as

$$[x]' = [\Delta\omega \quad \Delta\phi \quad \Delta E]^T \tag{33}$$

So that the state space matrix can be written as

$$A' = \begin{bmatrix} a'_{11} & a'_{12} & a'_{13} \\ 1 & 0 & 0 \\ 0 & \beta_3 & \beta_4 \end{bmatrix} \tag{34}$$

Hence the system response can be investigated through root locus plots defined by (6), (28) and (34). The parameters of converters are selected as shown in Table IV. Fig. 9 depicts the root locus diagram with the system operating in two modes where *MD*=0 and *MD*=1, respectively. It shows that when the system operates in VCM and *MD*=0, the three poles (P_1, P_2 and P_3) deduced from (34) mainly determine the dynamic response. When the unit changes to work in PCM and *MD*=1, these three poles become less dominant and the additional pole (P_4) activated by the integral term m_i turns into dominant pole. In both modes, the system is stable in the range of concern since the poles traces remain in the left half *s*-plane. Fig. 10 shows the root locus of system with the increasing of m_i when *MD*=1. It presents that the m_i should be selected in a suitable range ($0<m_i<0.135$) to avoid poles going into the unstable region. Although increasing m_i can reduce the steady state error of power regulation under PI controller, a high integral term can result in a sharp bus frequency change when all VCM units change to PCM modes. Therefore a smaller value than the boundary of m_i (m_i=0.135) can be selected to moderate the modes changing process when tuning system performance. Fig.

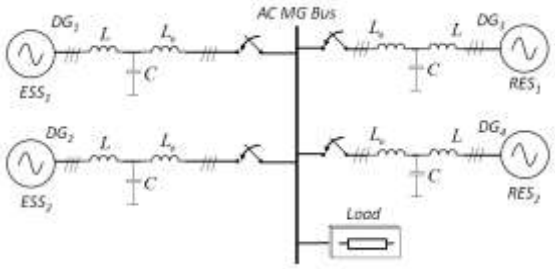

Fig. 16. System configuration of simulation.

11 shows the root locus of system considering variation of m_p. With m_p increasing, the pole (P_4) is attracted toward the origin and becomes more dominant. It can be seen that by increasing proportional term m_p of droop controller, the system dynamic performance can be improved for power regulation. However, as larger value of m_p results in severer bus frequency deviation in steady state, the selection of m_p should take into account the tradeoff between the good dynamic and steady state system response. It can be referred to [22] for more detailed description of parameters selection of PI droop controller. Fig. 12 and Fig. 13 show the root locus of system with the increase of n_p ($0.01 \le n_p \le 0.1$) with different values of *MD*. Since these dominant poles in both situations have little variation with increase of n_p, it can be concluded that compared with other parameters, the variation of n_p has little effect on the system dynamic response. Fig. 14 and Fig. 15 show the root locus with the variation of m_d ($0.000025 \le m_d \le 0.00025$) with different values of *MD*, the figures show that the increase of derivative term in both cases can increase the system damping in dynamic response. While it is worth noticing that this derivative term can be omitted in practical digital control system due to its sensitiveness of noises.

TABLE IV
POWER STAGE AND CONTROLLER PARAMETERS

Parameter	Symbol	Value	Unit
Power Stage			
Nominal Voltage Amplitude	V^*	230	V
Nominal Bus Frequency	f^*	50	Hz
Filter Inductance	L	1.8	mH
Filter Capacitance	C	27	μF
Output Inductance	L_o	1.8	mH
Linear Resistive Load	R_L	100	Ω
Inner loop Control			
Voltage Loop PR	k_{pV}, k_{iV}	0.1, 200	-, s^{-1}
Current Loop PR	k_{pI}, k_{iI}	20,1000	-, s^{-1}
Virtual Impedance	R_v, L_v	1, 4	Ω, mH
Primary Control			
Proportional Frequency Term	m_p	0.004	rad/(W·s)
Integral Frequency Term	m_i	0.02	rad/(W·s^2)
Derivative Frequency Term	m_d	0.0002	rad/(W)
Voltage Amplitude Term	n_p	0.025	V/(Var·s)
Maximum Power of RES	P_1^*, P_2^*,	1.0, 1.5	kW
Frequency Up-threshold	ω_{up}	51·2π	rad
Frequency Low-threshold	ω_{low}	50·2π	rad

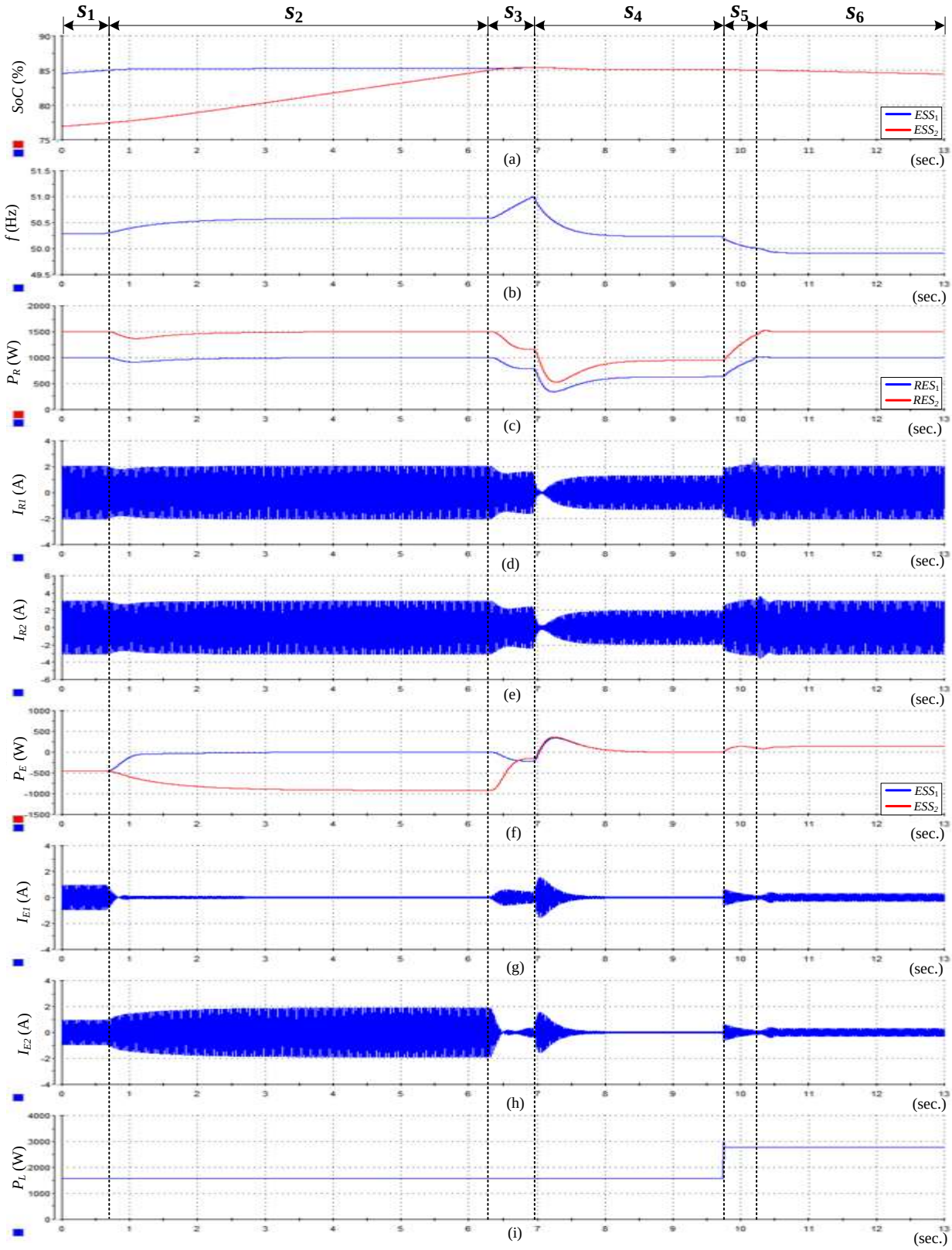

Fig. 17 Simulation results of four modes operation and transfer procedures

VI. HARDWARE-IN-THE-LOOP RESULTS

In order to verify the proposed SSDC control, real-time HiL simulations are carried out based on dSPACE 1006. The real-time simulation model which comprised of four inverters with LCL-filters is shown in Fig. 16. The AC islanded microgrid model consists of two ESS units and two RES units operating in both VCM and PCM based on SSDC. The power stage and control parameters are shown in Table IV. The parallel inverter model is established in MATLAB/Simulink and then downloaded into dSPACE 1006. In this way, the time span in

the simulation equals to that in the real system, e.g. 1-second simulation is finished in 1-second.

Under this test system, the proposed control strategy is for simplicity implemented on sole voltage source converters. However, when considering specific practical applications, multi stage converter systems can be used in order to incorporate this strategy on real RES units such as PV arrays or small wind turbines with permanent magnet synchronous generators [32]. In that case RES generator side converter typically performs maximum power point tracking algorithm, while grid side converter regulates intermediate DC link voltage to inject all available power to the grid. When reduction of output power is required, i.e. in stand-alone mode, DC link chopper is commonly incorporated to dissipate the excess of power [32]. It should be noted that DC link voltage and PQ regulation loops can be used together and the control strategy proposed in this paper can then be directly applied. However, since detailed analysis of MPPT algorithm is out of scope of this paper, an intermediate DC link is considered here to be a stiff voltage source and a constant power generation determined by P^* (see Fig. 8(b)) is used to represent the behavior of RES units when the converter is operating in PCM mode. Here P^* represents the maximum available power from RES which can be calculated in real system either in open loop according to environmental conditions or reached automatically by aforementioned control of back to back converter system. The nominal power ratings of RES units that correspond to P^* are set as 1kW and 1.5kW, respectively. Moreover, since this paper focuses on active power regulation taking into account of SoC condition, the load is modeled as resistive linear load with constant power consumption as shown in Table IV.

The simulation results of four operational modes and transfer procedures are shown in Fig. 17. In Fig. 17, (a) presents SoC of ESS units and (b) shows AC bus frequency, (c) and (f) show the power of RES units and ESS units respectively, (d) and (e), (g) and (h) shows the output currents of RES units and ESS units respectively, and (i) presents the power of loads. The scenario of four operational modes is summarized as:

- Scenario S_1: Both ESS_1 and ESS_2 are not fully charged, which indicates the SoC of both ESS are below 85% (Fig. 17(a)). The overall system operates in Mode I with ESS units controlled in VCM (Fig. 17(f)) and RES units in PCM with 1kW and 1.5kW respectively (Fig. 17(c)).
- Scenario S_2: The SoC of ESS_1 reaches 85%, so that it changes to operate in PCM. However ESS_2 is not fully charged and it starts to increase the charging rate as a result of power limitation of ESS_1. The system keeps operating in Mode I because ESS units have capability to regulate power of loads.
- Scenario S_3: Both SoC of ESS_1 and ESS_2 reach up-threshold 85%, so that ESS_2 also changes mode to PCM to limit charging power (Fig. 17(f)) and system operates in Mode II. Due to bus-signaling effect, the bus frequency is increasing steadily in this period since power generation is larger than power consumption (Fig. 17(b)).
- Scenario S_4: The AC bus frequency reaches up-threshold 51Hz (Fig. 17(b)), both RES units receive the frequency signal for changing mode from VCM to PCM and decrease power generation to meet load demand 1.6kW, so that the system operates in Mode III.
- Scenario S_5: Load consumption increase from 1.6kW to 2.8kW (Fig. 17(i)), then ESS_1 and ESS_2 start to discharge power (Fig. 17(f)) and RES units increase power to support load change (Fig. 17(c)). As load increases, the bus frequency drops correspondingly (Fig. 17(b)). When bus frequency decreases to 50Hz, ESS units change mode back to VCM and then system changes to Mode IV.
- Scenario S_6: The power of RES units restore to 1kW and 1.5kW so that RES units change mode back to PCM (Fig. 17(c)). In this case, the overall system changes mode back to Mode I with ESS and RES units operating in VCM and PCM respectively.

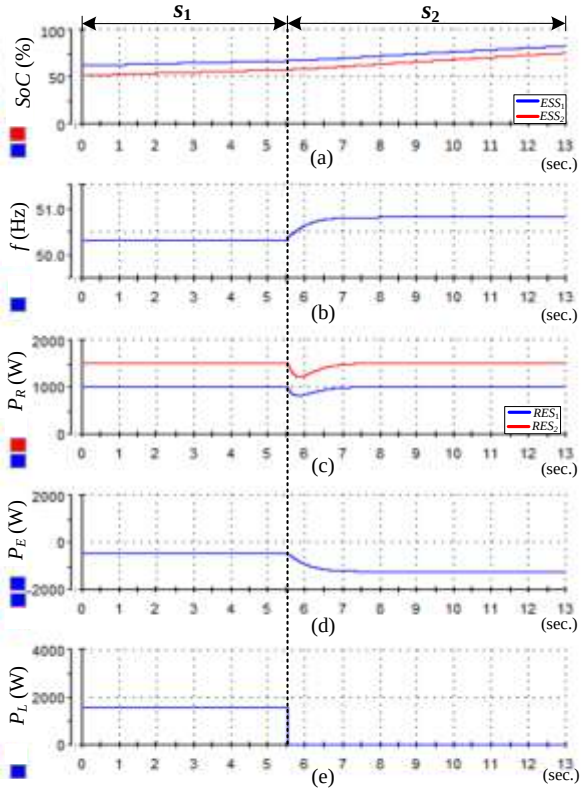

Fig. 18 System response due to sudden load outage when ESS not approaching to fully charged.

Fig. 18 investigates the microgrid performance when ESS not approaching to by fully charged, and the scenario of frequency increase due to a sudden load outage of overall system is presented. At 5.5s in Fig. 18, there is a sudden load outage from 1.6kW to 0 (Fig. 18(e)). Then the bus frequency increases from 50.3Hz to 50.8Hz (Fig. 18(b)). In both scenarios of S_1 and S_2, the SoC of ESS units are not approaching to be fully charged as shown in Fig. 18(a). It can be seen from simulation results that the overall system is able to achieve good power regulation response in dynamic process.

VII. Conclusion

This paper proposed a novel coordinated control strategy for AC islanded microgrids. In order to control flexibly the power of each unit, smooth switching droop control was implemented for each ESS and RES unit which adjusts droop slopes to switch modes between VCM and PCM. Based on SSDC, four operational modes and decentralized modes transition of system can be obtained. The coordinated control implementation was illustrated and small-signal analysis was carried out based on SSDC control. Finally the real-time hardware-in-the-loop simulation results verified the proposed coordinated control strategy by presenting the coordinated operation of system under different case scenarios.

References

[1] J. M. Guerrero, J. C. Vasquez, J. Matas, L. G. de Vicuna, and M. Castilla, "Hierarchical Control of Droop-Controlled AC and DC Microgrids—A General Approach Toward Standardization," *IEEE Trans. Ind. Electron.*, vol. 58, no. 1, pp. 158–172, Jan. 2011.

[2] M. H. Nehrir, C. Wang, K. Strunz, H. Aki, R. Ramakumar, J. Bing, Z. Miao, and Z. Salameh, "A Review of Hybrid Renewable/Alternative Energy Systems for Electric Power Generation: Configurations, Control, and Applications," *IEEE Trans. Sust. Energy*, vol. 2, no. 4, pp. 392–403, Oct. 2011.

[3] F. Giraud and Z. M. Salameh, "Steady-state performance of a grid-connected rooftop hybrid wind-photovoltaic power system with battery storage," *IEEE Trans.Energy Conv.*, vol. 16, no. 1, pp. 1–7, Mar. 2001.

[4] G. M. Tina and F. Pappalardo, "Grid-connected photovoltaic system with battery storage system into market perspective," in *Proc. IEEE Sustainable Alternative Energy PES/IAS Conf.*, 2009, pp. 1–7.

[5] P. F. Ribeiro, B. K. Johnson, M. L. Crow, A. Arsoy, and Y. Liu, "Energy storage systems for advanced power applications," *Proceedings of the IEEE*, vol. 89, pp. 1744–1756, 2001.

[6] B. S. Borowy and Z. M. Salameh, "Methodology for optimally sizing the combination of a battery bank and PV array in a wind/PV hybrid system," *IEEE Trans. Energy Conv.*, vol. 11, pp. 367–375, Jun. 1996.

[7] Y. Gurkaynak and A. Khaligh, "Control and Power Management of a Grid Connected Residential Photovoltaic System with Plug-in Hybrid Electric Vehicle (PHEV) Load," in *Porc. IEEE APEC'09 Conf.*, 2009, pp. 2086–2091.

[8] A. A. Al-Shamma'a and K. E. Addoweesh, "Optimum sizing of hybrid PV/wind/battery/diesel system considering wind turbine parameters using Genetic Algorithm," in *Proc. IEEE IPECon'2012 Conf.*, 2012, pp. 121–126.

[9] S. Adhikari and F. Li, "Coordinated V-f and P-Q Control ofSolar Photovoltaic Generators With MPPT and Battery Storage in Microgrids," *IEEE Trans. Smart Grid*, vol. 5, no. 3, pp. 1270–1281, May 2014.

[10] K. T. Tan, P. L. So, Y. C. Chu, and M. Z. Q. Chen, "Coordinated Control and Energy Management of Distributed Generation Inverters in a Microgrid," *IEEE Trans. Power Del.*, vol. 28, pp. 704–713, Apr. 2013.

[11] K. T. Tan, X. Y. Peng, P. L. So, Y. C. Chu, and M. Z. Q. Chen, "Centralized Control for Parallel Operation of Distributed Generation Inverters in Microgrids," *IEEE Trans. Smart Grid*, vol. 3, pp. 1977–1987, Dec. 2012.

[12] Jong-Yul Kim, Seul-Ki Kim, and Jin-Hong Jeon, "Coordinated state-of-charge control strategy for microgrid during islanded operation," in *Proc. IEEE PEDG'2012 Conf.*, 2012, pp. 133–139.

[13] Jong-Yul Kim, Jin-Hong Jeon, Seul-Ki Kim, Changhee Cho, June-Ho Park, Hak-Man Kim, and Kee-Young Nam, "Cooperative Control Strategy of Energy Storage System and Microsources for Stabilizing the Microgrid during Islanded Operation," *IEEE Trans. Power Electron.*,vol. 25, pp. 3037–3048, Dec. 2010.

[14] D. Papadaskalopoulos, D. Pudjianto, and G. Strbac, "Decentralized Coordination of Microgrids With Flexible Demand and Energy Storage," *IEEE Trans. Sustain. Energy*, vol. PP, no. 99, pp. 1–1, 2014.

[15] S. Bolognani, L. Peretti, L. Sgarbossa, and M. Zigliotto, "Improvements in Power Line Communication Reliability for Electric Drives by Random PWM Techniques," in *Proc. IEEE IECON'06 Conf.*, 2006, pp. 2307–2312.

[16] W. Stefanutti, S. Saggini, P. Mattavelli, and M. Ghioni, "Power Line Communication in Digitally Controlled DC–DC Converters Using Switching Frequency Modulation," *IEEE Trans. Ind. Electron.*, vol. 55, pp. 1509–1518, Apr. 2008.

[17] D. J. Perreault, R. L. Selders, and J. G. Kassakian, "Frequency-based current-sharing techniques for paralleled power converters," *IEEE Trans. Power Electron.*, vol. 13, no. 4, pp. 626–634, Jul. 1998.

[18] T. Dragicevic, J. M. Guerrero, and J. C. Vasquez, "A Distributed Control Strategy for Coordination of an Autonomous LVDC Microgrid Based on Power-Line Signaling," *IEEE Trans. Ind. Electron.*, vol. 61, no. 7, pp. 3313–3326, Jul. 2014.

[19] D. Boroyevich, I. Cvetkovic, D. Dong, R. Burgos, F. Wang, and F. Lee, "Future electronic power distribution systems a contemplative view," in *Proc. Int. Optimization of Electrical and Electronic Equipment Conf.*, 2010, pp. 1369–1380.

[20] J. Schonbergerschonberger, R. Duke, and S. D. Round, "DC-Bus Signaling: A Distributed Control Strategy for a Hybrid Renewable Nanogrid," *IEEE Trans. Ind. Electron.*, vol. 53, no. 5, pp. 1453–1460, Oct. 2006.

[21] J. M. Guerrero, L. GarciadeVicuna, J. Matas, M. Castilla, and J. Miret, "A Wireless Controller to Enhance Dynamic Performance of Parallel Inverters in Distributed Generation Systems," *IEEE Trans. Power Electron.*, vol. 19, , pp. 1205–1213, Sep. 2004.

[22] J. M. Guerrero, L. GarciadeVicuna, J. Matas, M. Castilla, and J. Miret, "Output Impedance Design of Parallel-Connected UPS Inverters With Wireless Load-Sharing Control," *IEEE Trans. Ind. Electron.*, vol. 52, pp. 1126–1135, Aug. 2005.

[23] J. Kim, J. M. Guerrero, P. Rodriguez, R. Teodorescu, and K. Nam, "Mode Adaptive Droop Control With Virtual Output Impedances for an Inverter-Based Flexible AC Microgrid," *IEEE Trans. Power Electron.*, vol. 26, no. 3, pp. 689–701, Mar. 2011.

[24] T. Dragicevic, J. M. Guerrero, J. C. Vasquez, and D. Skrlec, "Supervisory Control of an Adaptive-Droop Regulated DC Microgrid With Battery Management Capability," *IEEE Trans. Power Electron.*, vol. 29, no. 2, pp. 695–706, Feb. 2014.

[25] D. Martin, "Design of Parallel Inverters for Smooth Mode Transfer Microgrid Applications," *IEEE Trans. Power Electron*., vol. 25, no. 1, pp. 6–15, Jan. 2010.

[26] M. H. Nehrir, C. Wang, K. Strunz, H. Aki, R. Ramakumar, J. Bing, Z. Miao, and Z. Salameh, "A Review of Hybrid Renewable/Alternative Energy Systems for Electric Power Generation: Configurations, Control, and Applications," *IEEE Trans. Sustain. Energy*, vol. 2, no. 4, pp. 392–403, Oct. 2011.

[27] T. L. Vandoorn, J. D. M. De Kooning, B. Meersman, J. M. Guerrero, and L. Vandevelde, "Automatic Power-Sharing Modification of *P/V* Droop Controllers in Low-Voltage Resistive Microgrids," *IEEE Trans. Power Deliv.*, vol. 27, no. 4, pp. 2318–2325, Oct. 2012.

[28] W. Yao, M. Chen, J. Matas, J. M. Guerrero, and Z.-M. Qian, "Design and Analysis of the Droop Control Method for Parallel Inverters Considering the Impact of the Complex Impedance on the Power Sharing," *IEEE Trans. Ind. Electron.*, vol. 58, no. 2, pp. 576–588, Feb. 2011.

[29] D. Linden and T. B. Reddy, *Handbook of batteries*. McGraw-Hill, 2002.

[30] B. Xiao, Y. Shi, and L. He, "A universal state-of-charge algorithm for batteries," *Design Automation Conference (DAC), 2010 47th ACM/IEEE* , vol., no., pp.687,692, 13-18 June 2010.

[31] H. J. Avelar; W.A. Parreira, J. B. Vieira; L. C. de Freitas, E. A. Alves Coelho, , "A State Equation Model of a Single-Phase Grid-Connected Inverter Using a Droop Control Scheme With Extra Phase Shift Control Action," *IEEE Trans. Ind. Electron.*, vol.59, pp.1527,1537, March 2012.

[32] R. Teodorescu and F. Blaabjerg, "Flexible Control of Small Wind Turbines With Grid Failure Detection Operating in Stand-Alone and Grid-Connected Mode," *IEEE Trans. Power Electron.*, vol. 19, no. 5, pp. 1323–1332, Sep. 2004.